LRP 677/00 August 2000

Effect of $E \times B$ Flows on Global Linear Ion Temperature Gradient Modes

M. Maccio, J. Vaclavik, L. Villard

Submitted for publication in
Physics of Plasmas

ISSN 0458-5895

Effect of $E \times B$ Flows on Global Linear Ion Temperature Gradient Modes

M. Maccio, J. Vaclavik, L. Villard

Centre de Recherches en Physique des Plasmas, Association Euratom - Confédération Suisse

Ecole Polytechnique Fédérale de Lausanne, PPB - CH-1015 Ecublens/Switzerland

(August 25, 2000)

Abstract

Strong electric fields generate an $E \times B$ rotation of the equilibrium plasma. Experiments have shown that this effect could lower the anomalous transport in tokamaks. The study of the effect of these flows on the linear stability of ion temperature gradient (ITG) modes has therefore been undertaken. The question is addressed solving the spectrum of the gyrokinetic equation in the full two-dimensional poloidal plane. Results show a strong stabilizing effect of $E \times B$ flows on the ITG modes. Study with respect to different profiles of the flow shows that the so-called curvature of flow (second derivative) has no effect, while the intensity of flow itself produces the strongest effect. Study with respect to different magnetic shears did not allow to discover any particular behavior of the negative magnetic shear cases. Eventually, we conducted an experimental comparison with the Asdex Upgrade tokamak in Garching.

52.35.Kt, 52.25.Fi, 52.25.Dg, 52.35.-g

I. INTRODUCTION

$E \times B$ sheared flows are widely held responsible for the creation of internal transport barriers in fusion devices. Thus, the anomalous transport should be reduced as a consequence of their presence [1]. On the other hand, micro-instabilities are a major candidate to explain the anomalous transport. It is therefore natural to study the effect of $E \times B$ sheared flows on micro-instabilities and particularly on the linear stability of ion temperature gradient (ITG) modes, in a toroidal geometry.

Previous work [2] on this question has shown that the ballooning transform is of no use for this. The simplest way to avoid this problem is to study the effect of these sheared flows in the full two-dimensional poloidal plane. The first attempt to do so is a global and spectral fluid model [3] that addresses the question of the linear stability of ITG modes. This model has an important drawback: the lack of Landau damping, which allows plenty of slab-like ITG modes to exist even in the tokamak geometry. The slab-like modes being not strongly affected by the $E \times B$ flows, the results of the fluid model were rather disappointing, although a strong effect on the toroidal ITG modes could be seen, but not studied with much precision.

This motivated the present work, in which the same study is undertaken, but in the framework of the kinetic theory. We started from the gyrokinetic equation with strong electric fields that was obtained by Hahm [4] and solved it using the formalism developed by Brunner *et al.* [5]. This formalism solves the problem of linear stability of ITG modes in the full two-dimensional poloidal plane. It includes the effects of finite Larmor radius (FLR) to all orders in a spectral approach.

The article is organized as follows: in Sec. II A we explain how to include $E \times B$ flows in the resolution of the gyrokinetic equation. Then, in Sec. II B we restrict ourselves to a large aspect ratio tokamak. The numerical implementation is discussed in Sec. III. Eventually, in Sec. IV we present the results and discuss them.

II. GYROKINETIC MODEL

The plasma is modeled by gyrokinetic ions with full FLR effects and adiabatic electrons. We linearize the gyrokinetic equation for ions, including a strong equilibrium electric field. Then the quasi-neutrality approximation is used to couple the ions to the electrons, which are considered adiabatic or bounce averaged. This results in an eigenvalue integral equation for the ITG modes with strong electric fields. The spectral problem is solved in the full two-dimensional poloidal plane for a large aspect ratio tokamak.

A. General geometry

The first step is to include strong electric fields in the gyrokinetic formalism. This was done by Hahm [4] with the use of Hamiltonian mechanics in non-canonical variables and Lie transform formalism. We solve this new gyrokinetic equation using a perturbation method, as we are interested in the linear stability problem.

In [4], Hahm used the variables $\{\mathbf{R}, \alpha, \mu, v_{||}, t\}$, being the guiding center position, Larmor rotation angle, magnetic moment, parallel velocity and time, respectively. But to simplify our linear calculations, we have decided to work with an "energy" variable ε instead of the parallel velocity $v_{||}$, because, as we will see later, at the lowest order in perturbation, it is a constant. We define it as:

$$\varepsilon := e\phi_0 + m\mu B + \frac{m}{2}\left(v_{||}^2 + \mathbf{u}^2\right) \tag{1}$$

where e and m are the ion charge and mass respectively, ϕ_0 is the potential for the strong electric field, B is the modulus of the magnetic field, $\mathbf{u}$ is the sheared $E \times B$ flow:

$$\mathbf{u} := \frac{1}{B^2}\mathbf{B} \times \nabla\phi_0 \tag{2}$$

The second step is to apply an electrostatic perturbation $< \delta\phi >$ to the equilibrium plasma; the notation $< \cdots >$ represents an averaging over α, which appears via the Lie transform formalism. Given this, it is easily shown that:

$$\dot{\varepsilon} = -e\dot{\mathbf{R}} \cdot \nabla \left[< \delta\phi > (\mathbf{R}, \mu, t) \right] \tag{3}$$

where $\nabla = \partial_{\mathbf{R}}$ and we have [4]:

$$\dot{\mathbf{R}} = v_{\|}\mathbf{e}_{\|} + \mathbf{u} + \frac{1}{eB_{\|}^{\star}} \left[m\mu\nabla B + m\left(v_{\|}\mathbf{e}_{\|} + \mathbf{u}\right) \nabla \left(v_{\|}\mathbf{e}_{\|} + \mathbf{u}\right) \right] \tag{4}$$

where $B_{\|}^{\star} = B + (m/e)\mathbf{e}_{\|} \cdot \mathrm{rot}(v_{\|}\mathbf{e}_{\|} + \mathbf{u})$ and $\mathbf{e}_{\|} = \mathbf{B}/B$. It is possible to show, using the Lie transform formalism, that:

$$n_{ions}(\mathbf{x}, t) = \int B_{\|}^{\star} \left[F + \frac{e}{mB} \delta\tilde{\phi} \partial_{\mu} F + f \right] \cdot \delta(\mathbf{R} + \rho_L - \mathbf{x}) d\mathbf{R} d\alpha d\mu dv_{\|} \tag{5}$$

where $\mathbf{x}$ is the position of the particle and not the position of the guiding centers and with the following definitions: $\delta\tilde{\phi} = \delta\phi - < \delta\phi >$ and $\delta(\cdots)$ is the Dirac distribution.

With the $\{\mathbf{R}, \alpha, \mu, \varepsilon, t\}$ variables, the linearized gyrokinetic equation reads:

$$\partial_t f + \dot{\mathbf{R}} \cdot \nabla f = - \left[\frac{1}{B^2} \left(\mathbf{B} \times \nabla < \delta\phi > \right) \cdot \nabla F + \dot{\varepsilon} \partial_{\varepsilon} F \right] \tag{6}$$

where f is the first order perturbation part of the distribution function and F is the equilibrium part. We choose F to be a Maxwellian.

Eq.(6) can be formally solved by integrating over time along the equilibrium trajectories. To simplify the expressions, we first single out the adiabatic part of f, by defining the function g:

$$g := f - e < \delta\phi > \partial_{\varepsilon} F \tag{7}$$

which is the non-adiabatic part of the first order perturbation of the distribution function. We also use the fact that it is possible to write the electrostatic perturbation $< \delta\phi >$ as [5]:

$$< \delta\phi > (\mathbf{R}, \mu, t) = \exp(-i\omega t) \int_{\mathbb{R}^3} d\mathbf{k} \left[J_0(k_{\perp}\rho_L) \delta\hat{\phi}(\mathbf{k}) \exp(i\mathbf{k} \cdot \mathbf{R}) \right] \tag{8}$$

with $\omega \in \mathbb{C}$ representing the spectral approach and where $\delta\hat{\phi}(\mathbf{k})$ is the Fourier transform of the potential $\delta\phi(\mathbf{R}, \alpha, \mu)$, i.e. the electrostatic perturbation not averaged over α. The averaging over α is represented in the Bessel function.

Then the formal solution of Eq.(6) is:

$$g = -\frac{eF}{T_i}\int_{\mathbb{R}^3} d\mathbf{k}\left[J_0(k_\perp \rho_L)\exp\left(i\mathbf{k}\cdot\mathbf{R}(t) - i\omega t\right)(\omega - \omega^\star)\, i\mathcal{P}\cdot\delta\hat{\phi}(\mathbf{k})\right] \tag{9}$$

where T_i is the ion equilibrium temperature, J_0 is the Bessel function, $k_\perp$ the component of $\mathbf{k}$ which is perpendicular to the magnetic field, ρ_L is the ion Larmor radius and we have defined the following differential operator:

$$\omega^\star := -\frac{iT_i}{eB}\left[\mathbf{e}_n\cdot\nabla\left(\ln F\right)\right]\left[\mathbf{e}_b\cdot\nabla\right] \tag{10}$$

where $\mathbf{e}_n$ and $\mathbf{e}_b$ are the normal and binormal unit vectors respectively, defined with respect to the flux surfaces and the field lines of the magnetic field.

The propagator $\mathcal{P}$ is defined as [5]:

$$\begin{aligned}\mathcal{P}(\mathbf{R},\mathbf{k},\varepsilon,\omega) &:= \int_{-\infty}^{t} dt' \exp\left[i\mathbf{k}\cdot\left(\mathbf{R}(t') - \mathbf{R}(t)\right) - i\omega\left(t'-t\right)\right] \\ &= \int_{-\infty}^{t} dt' \exp\left[i\int_{t}^{t'}\left(\mathbf{k}\cdot\dot{\mathbf{R}}(t'') - \omega\right)dt''\right]\end{aligned} \tag{11}$$

At this point, we have a formal solution to the perturbation calculation. It is worth noting that this formal solution is nowhere explicitly modified by the strong electric fields. In fact, this solution is exactly the same as the one obtained by Brunner et al. [5]. The only effect of the strong electric field is to modify the equations of motion of the guiding centers, thus modifying the trajectories, which explicitly appear in Eq.(11). Thus, all the details of the numerical resolution of the problem will be the same as in [5]. We only need to compute an explicit formula for the propagator with strong electric fields.

B. Large aspect ratio tokamak

We have restricted ourselves to the case of a large aspect ratio tokamak, with circular concentric flux surfaces. The magnetic field is taken as:

$$\mathbf{B}\left(\rho,\theta\right) = B_0\frac{R_0}{r(\rho)}\left(\mathbf{e}_\varphi + \frac{\rho}{R_0 q_s(\rho)}\mathbf{e}_\theta\right) \tag{12}$$

where R_0 is the major radius, $r(\rho) = R_0 + \rho\cos(\theta)$ is the cylindrical radius, B_0 is the magnetic field on the axis, $\mathbf{e}_\varphi$ is the unit vector along the toroidal angle, $\rho \in [0, a]$ is the minor radius,

θ is the geometric poloidal angle, $q_s(\rho)$ is the safety factor, which is chosen arbitrarily, and $\mathbf{e}_\theta$ is the unit vector along the poloidal angle. We assume that $a/R_0 \ll 1$.

The last step before the explicit computation of the propagator, is the determination of the equilibrium trajectories of the guiding centers, i.e. the computation of $\mathbf{R}(t')$. To solve the equations of motion, we use an iterative method, considering that the drifts are a correction to the unperturbed trajectories. In this geometry, the equilibrium equations of motion for the guiding centers read [Eqs.(4) and (12)]:

$$\begin{aligned}
\dot{\rho} &= -v_D \sin\theta + \frac{u^2(\rho)}{R_0\omega_{ci}} \sin\theta \\
\dot{\theta} &= \tilde{\omega}_t - \frac{v_D}{\rho}\cos\theta - \frac{u^2(\rho)}{\rho^2\omega_{ci}} \\
\dot{\varphi} &= \omega_t q_s(\rho)
\end{aligned} \tag{13}$$

where $\omega_t := v_\parallel/R_0 q_s(\rho)$ is the poloidal transit frequency and $\tilde{\omega}_t := \omega_t + u(\rho)/\rho$, ω_{ci} is the ion cyclotron frequency, $\{\rho, \theta, \varphi\}$ are the toroidal variables, and v_D is the magnetic drift:

$$v_D = \frac{1}{R_0\omega_{ci}}\left(B_0\mu + {v_\parallel}^2\right) \tag{14}$$

and $u(\rho)$ is obtained through (2) and (12):

$$\mathbf{u} = u(\rho)\left[1 + \frac{\rho}{R_0}\cos\theta\right]\mathbf{e}_\theta \tag{15}$$

From now on we will only consider highly passing ions and in order to solve the equations of motion, we will make the assumption that the parallel velocity is constant: $v_\parallel(t) = v_\parallel(t_0)\ \forall t$. Solving iteratively Eqs.(13) yields:

$$\begin{aligned}
\rho(t') - \rho(t) &= \frac{1}{\tilde{\omega}_t}\left(v_D - \frac{u^2}{R_0\omega_{ci}}\right)\left[\cos(\tilde{\omega}_t t') - \cos(\tilde{\omega}_t t)\right] \\
\theta(t') - \theta(t) &= \tilde{\omega}_t(t'-t) - \frac{u^2}{R_0\omega_{ci}}(t'-t) - \frac{v_D}{\rho\tilde{\omega}_t}\left[\sin(\tilde{\omega}_t t') - \sin(\tilde{\omega}_t t)\right] \\
\varphi(t') - \varphi(t) &= \omega_t q_s(t'-t)
\end{aligned} \tag{16}$$

These equations are what we were seeking: we can now safely proceed to the explicit computation of the propagator.

Before going further, we would like to point out that we have in fact used a toroidal wave decomposition rather than the standard plane wave representation. Thus, Eq.(8) should read:

$$\int_{\mathbb{R}^3} d\mathbf{k} \left[\delta\hat{\phi}(\mathbf{k}) \exp(i\mathbf{k}\cdot\mathbf{R})\right] = \sum_{k,m\in\mathbb{Z}} \delta\hat{\phi}_{(k,m)} \exp\left[i\left(k\frac{2\pi}{\Delta\rho}\right)\rho + im\theta + in\varphi\right] \tag{17}$$

where $\Delta\rho = (\rho_{Max} - \rho_{min})$ and $[\rho_{min}, \rho_{Max}]$ are the boundary within which we solve the problem. m and n are the poloidal and toroidal wave numbers, respectively, and $n \in \mathbb{Z}$ is fixed because the problem is axisymmetric. This decomposition implies an approximation on the geometry, which implications are fully discussed in [6].

Therefore, using Eq.(11), the iterative integration of the guiding centers trajectories and (17), it can be shown that the propagator becomes:

$$\mathcal{P}(\theta) = \sum_{p,p'\in\mathbb{Z}} J_p(x) J_{p'}(x) \frac{\exp\left[i(p-p')(\theta+\bar{\theta})\right]}{i\left(y - \omega + p\tilde{\omega}_t\right)} \tag{18}$$

where J_p are the Bessel functions and we have used the following definitions:

$$\begin{aligned}
x &= \left[\left(k\frac{2\pi}{\Delta\rho}\right)^2 \frac{1}{\tilde{\omega}_t^2}\left(v_D - \frac{u^2}{R_0\omega_{ci}}\right)^2 + \left(\frac{mv_D}{\rho\tilde{\omega}_t}\right)^2\right]^{\frac{1}{2}} \\
y &= m\tilde{\omega}_t + nq_s\omega_t - m\frac{u^2}{\rho^2\omega_{ci}} = k_{||}v_{||} + m\frac{u}{\rho}\left(1 - \frac{u}{\rho\omega_{ci}}\right) \\
\cos\bar{\theta} &= \left(k\frac{2\pi}{\Delta\rho}\right)\frac{1}{\tilde{\omega}_t}\left(v_D - \frac{u^2}{R_0\omega_{ci}}\right)/x \\
\sin\bar{\theta} &= \left(\frac{mv_D}{\rho\tilde{\omega}_t}\right)/x
\end{aligned} \tag{19}$$

where $k_{||} := (m+nq_s)/(R_0q_s)$. Eq.(18) is all we needed: it is the expression of the propagator in presence of a strong electric field. The set of equations is now complete: using (5), (7), (9), (18), the quasi-neutrality approximation and the adiabatic or bounce averaged electrons, we can produce an eigenvalue integral equation which considers the full 2-D poloidal plane. It can be solved to determine the spectrum of the ITG modes in the framework of gyrokinetic theory. The details are to be found in [5].

III. NUMERICAL IMPLEMENTATION

To give a resume, we have solved the linearized gyrokinetic equation for ions, in a spectral approach. This solution coupled with the adiabatic electrons gives rise to an integral equation for the eigenmodes of the electrostatic potential. The free input data parameters for our problem are: the profiles of equilibrium quantities, the parameters of the equilibrium geometry, the toroidal wave number n, and the profile of the $E \times B$ sheared poloidal flow u. Given these, the task is to find the eigenmodes of the plasma, i.e. find the values of ω for which there is a non-trivial solution $\delta\hat{\phi}$ to the integral equation.

We will not discuss in details the numerical approach, because it is rigorously the same as the one in Ref. 5. Indeed, we did not start from scratch, but had simply to modify the already existing and extensively benchmarked [7] GLOGYSTO code. The modifications we had to include did not request a modification of any of the numerical tools used. To put it simply, they only changed the function we had to integrate. The main modification comes from a symmetry breaking, that occurs in the integration over $v_{||}$, due to the flow. Indeed, the original formulation did an explicit use of the $v_{||} \to -v_{||}$ symmetry in the precalculation part [5]. We therefore had to, roughly speaking, double the memory use. Altogether, doing things properly, this did not result in a problem.

It must also be stressed that the GLOGYSTO code includes the possibility to study both adiabatic and trapped electrons, with a bounce averaged equation for the trapped ones. This part did not change, because we did not consider the effect of $E \times B$ flows on electrons, as it is smaller than the one on ions by a mass ratio factor. Therefore, although we did not present the equation, we have the possibility to include trapped electrons in our system [5].

Nevertheless, for those not acquainted with Ref. 5, we give here a brief account of the numerical methods. As noted in Eq.(17), the two space dimensions are decomposed on the Fourier functions basis. For the determination of the significant Fourier components to include in the computation, one should read Ref. 5, but the main argument remains naturally the convergence. The radial integration is performed on an equidistant mesh using the FFT

algorithm. The velocity integrals are not performed on the whole $\mathbb{R}^3$, but reduced to a sphere of radius $n \cdot v_{thi}$. The extended trapezoidal rule is used for this integration.

At this point, there are two questions that need to be answered. Does the inclusion of $E \times B$ flows deteriorate the numerical convergence ? Are the observed effects of $E \times B$ flows physical or numerical ? This last question is answered extensively in Sec. IV, where we do a benchmark between our spectral code and a PIC code, which is a completely different numerical approach. As discussed later on in more details, the effect of $E \times B$ flows are the same in the spectral and PIC codes, therefore we can trust our model. The answer to the first question can convincingly be met by the Fig. 1, in which we see an eigenmode in the Fourier space. As the figure demonstrate, inclusion of $E \times B$ flow does not affect much the extent of the Fourier space required. Nevertheless, the presented inclusion of flow has a very strong stabilizing effect (factor three) and a large Doppler shift of the frequency.

There are two methods to find the eigenvalues in the complex plane. In fact, our problem, after discretization, can be written like this:

$$\sum_j M_{ij}(\omega) \cdot \delta\hat{\phi}_j = 0 \tag{20}$$

Therefore, our task is simply to find the zeros of the analytical function $f(\omega) := \det(M)$. This is done using two different methods, depending on the number of eigenvalues present in a region of the complex plane $\mathbb{C}$. If the number of zeros is small, typically less than three, there is a very fast and efficient method based on the Nyquist theorem [6], [8]. It usually requires the sampling of f on eight to twenty points on a Jordan curve enclosing the eigenvalues. Otherwise, we need to do a rectangular scan of $\mathbb{C}$, and then plot the contour lines for $\Re(f) = 0$ and $\Im(f) = 0$: the intersections of these contour lines are our eigenvalues. This method requires normally a sampling of f on a mesh of $25 \times 25 = 625$ points. As we see, there is more than an order of magnitude difference between the two methods, but one cannot always avoid using the scan.

Let us now say a word about the computer implementation. The GLOGYSTO code, originally written in Fortran 77, has been upgraded to Fortran 90 for the author convenience

and the sake of portability. NAG routines are used for the FFT routines and most of the special functions, while LAPACK routines are used for the matrix calculations. The code was used on the following platforms successfully: on the Silicon Graphics R10000 processor, on the Sun Microsystems Sparc Ultra-2 processor and on the Cray J90 supercomputer processor. There exists also a parallel version of the code, but most of the runs were performed using the single processor version due to a surcharge of the EPFL parallel machine.

IV. RESULTS

We will present the following studies:

- effect of different profiles of $E \times B$
- effect of $E \times B$ flows in combination with magnetic shear
- experimental comparison with the Asdex Upgrade tokamak

A. Various Profiles of $E \times B$ flows

In this section we will study how various profiles of $E \times B$ poloidal flows affect the ITG toroidal modes. To make it short, we will see that the shear of the poloidal rotation velocity has a stabilizing effect, but in no way is this effect stronger than the one due to the value of the poloidal rotation velocity. We will also see that the value of the second derivative of the poloidal rotation velocity is an irrelevant quantity.

For this study, we chose the following parameters: $a = 0.21[\text{m}]$, $R_0 = 1.19[\text{m}]$, $B_0 = 1[\text{Tesla}]$, $T_e = T_i = 1[\text{keV}]$, the ions were hydrogen, $q_s \in [1, 5]$ and $q_s \approx 2$ where the mode amplitude is maximum. The parameters are set so that the ITG toroidal modes are much more unstable than the ITG slab-like modes that exist even in toroidal geometry. In this study we are only interested in ITG toroidal modes.

We have now to decide what value of n we want to study. It seems to us natural to be mainly interested in the most unstable n of our system. We have therefore made a scan in

n in order to find the most unstable eigenmode, results being plotted in Fig. 2. Clearly, the most unstable mode is given by $n = 7$, thus we studied only this mode. This might look like an awkwardly low value of n, but it must be stressed that as our calculations are global, we can impose the value of ρ_L, but the value of $k_\perp$ is given by the results of the calculations and we know that the most unstable toroidal ITG mode will have $k_\perp \cdot \rho_L \approx 0.5$, thus the concept of "high n" is relative to the plasma studied.

Now we come to the choice of the $E \times B$ profile. We want to study the effect of constant and sheared poloidal rotations. Thus, we chose the profile of $E \times B$ in the following way:

$$\frac{u(s)}{s} = \text{Mach} \cdot v_{thi} \left[u_0 + u_1 s + u_2 s^2\right] \tag{21}$$

where v_{thi} is the ion thermal velocity and $s = \rho/a$ is the normalized radial variable. This allows us to study separately the effect of constant flow, constant shear of flow and non constant shear of flow.

It is well known that the radial profile of the ITG toroidal modes is determined by the logarithmic derivative of the ion temperature and the safety factor, the modes trying to maximize the drive of the temperature gradient, while minimizing their $k_\parallel$. It is also very well known that the ITG toroidal modes do balloon in the region of unfavorable magnetic curvature, that is around $\theta \approx 0$. From now on, we will use $\{s_o, \theta_o\}$ to name the normalized radius and poloidal angle where the mode amplitude is maximum.

We can now describe the shapes of $u(s)$ that we considered. There are three basic cases and they are chosen starting with the constant poloidal rotation velocity. We want $u(s)/s$ to be equal to 1 and therefore, we took: $u_0 = 1, u_1 = 0, u_2 = 0$. we will call this profile "constant flow". Then, we want to "normalize" the values of the first and second derivatives, therefore we choose profiles such that $\partial_s(u(s)/s) = 1$ and $\partial_s^2(u(s)/s) = 1$ everywhere. Therefore, the second shape, that we will call "constant shear", is thus given by: $u_0 = -s_o$, $u_1 = 1$, $u_2 = 0$; the flow vanishes at s_o, but it has constant shear. And the third shape, that we will call "non constant shear", is given by: $u_0 = \frac{1}{2}s_o^2$, $u_1 = -s_o$, $u_2 = \frac{1}{2}$. The flow and its constant shear both vanish at s_o, but the profile being parabolic, the second derivative of flow is not

vanishing there. The three profiles are plotted in Fig. 3. For each of them, the "driving terms" (the value of $u(s)/s$, the first derivative of $u(s)/s$ and the second derivative of $u(s)/s$ respectively) have all the same value at s_o: Mach $\cdot\, v_{thi}$.

Let us first see the effect of the $E \times B$ flow on the frequency ω and growth rate γ of a toroidal ITG mode. Results are shown in Fig. 4 and Fig. 5 where we can compare the different profiles of flow. The evolution of the frequencies is easily understood: for the constant flow case, we see a simple Doppler shift of the frequency, while for the other two cases we see that the frequency is unaffected. This is normal, as for these two cases there is no effective value of flow at s_o. Let us now have a look at the growth rates. We clearly see that the most stabilizing effect is due to the constant flow profile, while the constant shear is also strongly stabilizing. On the other hand, the second derivative of flow is completely ineffective: it does not at all affect the mode. We will explain the mechanism that leads to the observed stabilizations, but we would first like to offer a validation of our results.

We have two validations for these results: a comparison with a local dispersion relation and a benchmark with a global PIC code, which are shown in Fig. 6. Let us begin with the local dispersion relation. A kinetic local dispersion relation has been derived by Brunner [5] for the study of the ITG modes without flow. The introduction of flow can simply be seen as a Doppler shift in the frequency, given by Mach $\cdot\, v_{thi} \cdot k_\theta \cdot u(s_o)$ Therefore, in cases where $u(s_o) = 0$, one expects no variation of the frequency and this is exactly what is observed for both the constant shear case and non-constant shear case. For the constant flow case, one expects a Doppler shift and one can compare the global spectral code with the dispersion relation. This is done in Fig. 6. To have a benchmark for our growth rates, we did a comparison with a PIC code [9], modified by L. Villard to include $E \times B$ flows. The results of the PIC code are also shown in Fig. 6. They are in excellent qualitative agreement with the results of the spectral code. The values of the frequencies are perfectly matching, while the values of the growth rates have a perfectly similar functional dependence on the Mach number, although the values are only in an agreement of 20%. This discrepancy does exist even for a vanishing Mach number and is simply explained by the different approximations

used by both codes. For instance, the PIC code does not have an exact resolution of the linearized gyrokinetic equation to all orders in Larmor, while the spectral code does. For a detailed discussion of these issues see [7]. It is simply important to know that this discrepancy is not due to $E \times B$ flows.

One legitimate question is whether we are following one particular mode in our scans in Mach number or if we are checking the whole complex plane. To this question, it must be answered that checking the "whole" complex plane is by no means possible, but the comparison with the PIC code, which is only able to produce the most unstable ITG mode in the system, shows that there are no new unstable modes popping out. This is normal, as we chose our parameters so that there would be only a strongly unstable ITG toroidal mode, while there are some other modes, but much less unstable. Therefore in Fig. 4 and Fig. 5 it must be considered that we plot the evolution of the most unstable mode.

Now, we would like to discuss the mechanism of stabilization. In Fig. 7 we show the effect of $E \times B$ flows on the poloidal contour plots of the electrostatic potential. The constant flow case is presented in the left column, while the constant shear case is in the right column. As one sees, there is not much qualitative difference between the two cases, the constant shear case needing simply a larger value of the Mach number. Before going further, it is important to stress that due to a convention in the code, a positive Mach number refers to plasma rotation in the clockwise direction.

Let us begin with the "constant flow" case: left column of Fig. 7. It is obvious that the mode is simply rotated along with the plasma, that is the region θ_o where the mode balloons is moved. The consequence of which is to move the mode maximum amplitude region away from the unfavorable magnetic curvature region, reducing therefore the instability. A negative Mach number means a poloidal flow going upward on the external side of the plasma. Thus, for low negative values of Mach number, θ_o is first moved to a more unfavorable position, thus destabilizing the ITG. But, for stronger Mach number, θ_o moves further, leaving the unfavorable region, finally producing a strong stabilization of the toroidal ITG. This effect is naturally only effective for toroidal ITG modes, as the unfavorable magnetic

curvature is for them necessary, while slab ITG modes can live without it.

Now, let us have a look at he "constant shear" profile, that is the right column of Fig. 7. It is difficult to see much difference with the "constant flow" case. It looks like if the mode, being global, had to choose between one of the sides of the flow and chose the external rotation, thus being affected like by the value of flow. The main difference being now that of course, the value of flow is not the same as before, resulting in different values of Mach numbers.

Now, coming back to Fig. 5, we see that the "non constant shear" has clearly no relevant effect. This is in contradiction with most models, but assuming that our explanation of the mechanism of stabilization is correct (that is: the mode is stabilized because it is removed from the region of unfavorable magnetic curvature), then the non-effect of non-constant shear is obvious, as looking at Fig. 3 clearly shows that the value of flow is almost zero everywhere for this case.

Now we would like to briefly describe the effect of the $E \times B$ flow on $k_\perp$, and $k_\parallel$ that we can estimate by averaging over the eigenmode: $k_\perp^2 = \langle \nabla_\perp \delta\phi^* \cdot \nabla_\perp \delta\phi \rangle / \langle \delta\phi^* \delta\phi \rangle$ and $k_\parallel^2 = \langle \nabla_\parallel \delta\phi^* \cdot \nabla_\parallel \delta\phi \rangle / \langle \delta\phi^* \delta\phi \rangle$. The results are plotted in Fig. 8. We see that the variations of $k_\perp$ and $k_\parallel$ are exactly matching the variations of γ: when the mode gets stabilized, both $k_\perp$ and $k_\parallel$ are increasing and for the small region where the mode gets more unstable, both $k_\perp$ and $k_\parallel$ are decreasing. Although the absolute increase in $k_\perp$ is small, it nevertheless goes in the "good direction", that is it tends to reduce the linear estimate for the diffusion coefficient $D = \gamma / k_\perp^2$.

B. Various Magnetic Shears

It is often claimed that negative magnetic shear should be a main component of the ITB creation. Nevertheless, Brunner noticed [5] that with our model negative magnetic shear on its own does not exhibit a spectacular effect, but of course, that was done without $E \times B$ flows. Now the question arises, can $E \times B$ flows interact with a negative magnetic shear so

as to produce a synergic effect ?

In order to answer this question, we have chosen the following physical system: $a = 0.5$[m], $R_0 = 2$[m], $B_0 = 1$[Tesla], $T_e = T_i = 2.13$[keV], the ions are hydrogen, $q_s(s_o) = 1.5$ and the most unstable mode is found for $n = 10$. Then, as we did in the fluid case, we have kept the value of $q_s(s_o)$ constant while changing the value of magnetic shear (simply called shear from now on) $s_o \cdot d_s q_s(s_o)/q_s(s_o)$. We considered the following values for the shear: $\{-1, 0, +1\}$. This study, without $E \times B$ flows, had been already done by Brunner [5]. The qualitative nature of the modes changes for the three cases as is to be observed in Fig. 9. The positive shear case clearly exhibits a toroidal nature, while the negative shear mode does not balloon and is therefore more of a slab nature. As expected, the vanishing shear case is somewhere in between the two other cases.

We now have to choose the profile of $E \times B$ flow that will interest us: we decided to study the effect of the "constant shear" (see Eq.(21)) profile on the various values of shear, because it is the most popular one in the literature. In Fig. 10 we present the evolution of the complete spectrum for increasing values of Mach number.

Let us now discuss the results. As is easily observed, the negative shear case is the one presenting the largest number of eigenmodes. This can be understood due to the slab-like nature of these modes. Besides, these modes are clearly less unstable than the other two cases modes, even without flow. But it must also be observed that the effect of $E \times B$ flows in the negative shear case is small. On the other hand, the positive shear case has only a few unstable modes, most of which are quickly stabilized. The no shear case has also only a few unstable modes, most of which are also quickly stabilized, but the most unstable mode in this case is not very strongly affected by flow. These comments are summarized in Fig. 11, where we plotted only the evolution of the most unstable mode, for the three considered cases. One clearly sees that the negative shear mode stays almost unaffected, while the positive magnetic shear mode is strongly damped. The different evolutions of the frequencies are to be understood by the fact that the radial localization of the modes is not exactly the same for the various shears and therefore the value of flow seen by the mode is

slightly different in each case.

How can we understand the observed differences ? If our explanation of the stabilizing mechanism has to be correct, then the differences can be understood in the following way: the positive shear case is a toroidal ITG mode, as it is removed from the region of unfavorable magnetic curvature, its drive is reduced and the mode gets stabilized. On the other hand, the slab-like nature of the negative shear mode allows it to survive without the magnetic curvature, therefore a rotation of this mode will not affect much its growth rate. The conclusion of this study is therefore that there is no synergy between negative shear and $E \times B$ flows.

We would like to say a last word about what could happen if we took negative Mach numbers. The answer is 'nothing particular'. Indeed, as we learned with the first results, there is not much difference on stabilization for different signs of Mach number, the orders of magnitude being exactly the same. Moreover, our interpretation of why the negative magnetic shear mode is not strongly affected is that, because of its slab-like nature, its rotation in the poloidal plane does not affect much its drive. This would remain true even if we rotated it in the opposite direction.

C. Asdex Upgrade Comparison

We have decided to study an experimental configuration with our global spectral code. To achieve this, we have collaborated with people of the Asdex Upgrade (AUG) tokamak, in Garching. In particular, the following results would never have been possible without the kind cooperation of Arthur Peeters and Sibylle Günter of the Max Planck Gesellschaft.

There are two main features to keep in mind for this experimental case. First the shot had an Internal Transport Barrier diagnosed by the AUG experimentalists, which means that the confinement was improved. As we claim that $E \times B$ flows can stabilize microinstabilities, it is thus a good case for us. Second, this case is an ITG mode destabilized by trapped electrons. It is not a pure TEM, because it is still on the frequency side of the ITG modes,

but without trapped electrons it would be completely stable.

1. Equilibrium

We had a choice of several AUG shots where experimentalists had diagnosed an Internal Transport Barrier (ITB). After a little investigation we found a shot which seemed to be an excellent candidate. The experimental reconstructed profiles were introduced as input parameters in our code. The critical profiles are to be seen in Fig. 12. The following parameters are also important: $a = 0.51$[m], $R_o = 1.65$[m], $B_o = 2.61$[Tesla], $T_e = 4.56$[keV], $T_i = 13.72$[keV] and the ions are deuterium. One must still decide which n to study: we did a scan in n and took the most unstable mode, which resulted to be $n = 15$.

These profiles seemed to be smooth enough to avoid numerical problems and had perfectly adequate values of η_e and η_i. Nevertheless, at the beginning we ran into some problems. Indeed, we were first not able to locate any unstable modes, because we had not included the trapped electrons into our calculations. In Fig. 13, we explain what happens: the experiment has a value of $\tau = T_e/T_i = 0.332$, that is the ion temperature is roughly three times the electron temperature. Using this value, we did not find any unstable modes, even without $E \times B$ flows. Thus we decided to start with $\tau = 1$ (increasing the electron temperature T_e) and we were then able to find unstable modes. Starting with these modes, we progressively reduced the electron temperature T_e until we reached the experimental value of τ. This resulted in a fast stabilization of the modes. Hopefully, the inclusion of trapped electron effects, starting with $\tau = 1$ and evolving to $\tau = 0.3$, allowed us to find unstable modes even at the experimental value of τ.

This discussion is not meaningless, because it is important to remember that up to now we did only study how $E \times B$ flows affected the pure ITG modes. This is a case where the main driving force for the instability are the trapped electrons, although this is not a trapped electron mode, as the sign of the frequency did not change.

2. Spectrum

We can now show how the $E \times B$ flows affect the AUG spectrum. In Fig. 14 we present the complete spectrum of the AUG case, with trapped electrons, for three increasing values of Mach number. It is clear that the number of modes is decreasing with increasing Mach number, as is the maximum growth rate. It must be stressed that in this particular case, the most instable mode is not always the same. This is due to the fact that the various unstable modes do not have the same radial profile and thus do not see the same part of the $E \times B$ profile. This results in Doppler shifts of various amplitudes, and the stabilizing mechanisms, whether the value of flow or its first derivative, are different for each mode.

In Fig. 15 we present the most unstable mode in the poloidal plane, with and without $E \times B$ flows. As we see, the ballooning region θ_o is not rotated in this case. Therefore our previous argument to explain stabilization seems no longer valid. First, let us remember that we are not observing the same mode in the two pictures: each mode is the most unstable for the given Mach number, but these are two different modes. Thus, it might be that for one given mode the θ_o region changes, but that the most unstable mode has it always close to $\theta \approx 0$. Second, we must remember that the modes we are studying are not pure ITG modes, as if we had not included the trapped electrons, the spectrum would have been stable. Therefore, as $E \times B$ flows have been neglected in the construction of the trapped electron contribution (due to the mass ratio), it is by no means simple to understand how they affect the present modes. To be clear, the $E \times B$ flows affect only the passing ions contribution to the mode, but without the trapped electron contribution there would be no mode. But the passing ions contribution is also essential to the mode, as it is not a TEM mode, but an ITG mode destabilized by trapped electrons. Therefore, it might well be possible that the poloidal structure of the mode is dictated by the trapped electrons, thus barely affected by $E \times B$ flows. But $E \times B$ flows still stabilize the mode, because they reduce the passing ions contribution, which is also essential to the existence of the mode.

Let us now come to the comparison with the experimental observations. With our results

we seem to observe that for a theoretical value of Mach number close to 0.03:

$$\text{Mach}_T \approx 0.03 \tag{22}$$

we will have completely stabilized the AUG spectrum. Now comes the question of how large is the experimental value of Mach number. It turns out that the measured Mach number is:

$$\text{Mach}_E = 0.0635 \tag{23}$$

As a first comment, we would like to say that it was already very good news to discover that the orders of magnitude were right. Then, we would stress another point: the theoretical value of Mach number represents the value by which the linear microinstabilities should be stabilized, it does not represent a maximum on the value of Mach number. What we mean is that it would have been more annoying if the theoretical value had been larger than the experimental one, as then experimentalists would claim an ITB where theorists would see none. But in our case, there is no argument why the Mach number could not be larger than the minimal stabilization value, represented by the theoretical value. Moreover, there are many limitations in both theory and experiment.

Theory is limited by:

- unrealistic shape of the equilibrium, which strictly speaking is not even an MHD equilibrium
- only linear calculations
- no electromagnetic effects
- the other (less obvious) approximations used in the code

Experimental values must be taken with care:

- an error bar of 20% on the ion temperature gradient
- an error bar of 40% on the $E \times B$ flows

3. *Empirical Criterium*

Our comparison with the AUG tokamak has led Arthur Peeters to propose an empirical criterium which should offer an estimate for the Mach number that is needed in order to stabilize the ITG modes. This criterium is to be used with cases in which the stabilization mechanism is not the shear of flow, but rather the value of flow.

The idea is simple enough: assuming that to become instable, a mode needs to spend at least a period $1/\gamma$ in the region of unfavorable magnetic curvature, we say that the mode would be stable if the poloidal rotation $u(\rho)/\rho$ happens to be faster. Explicitly, the criterium claims a stabilization if the following condition is fulfilled:

$$\frac{u(\rho)}{\rho \cdot \gamma} > 1 \tag{24}$$

using our normalization, we have: $u(\rho) = Mach \cdot v_{thi} \cdot u_o$, $\rho = a \cdot s_o$ and $\gamma = (v_{thi} \cdot \rho_{Li}/a^2) \cdot \gamma_o$, which leads to the following empirical criterium:

$$Mach > (\rho_{Li}/a) \cdot (\gamma_o s_o/u_o) \tag{25}$$

for a complete stabilization. Applying this criterium to the AUG comparison, we find that the criterium predicts a stabilization for a Mach number equal to 0.31, largely overestimating the result. Nevertheless, we should not forget that the AUG modes are mainly destabilized by TEM. Thus, applying the same criterium to the "constant flow" case presented in Sec. IV A, we find that it predicts a complete stabilization for a Mach number equal to 0.0168. This value is in excellent agreement with the global code results. This criterium has to be tested more extensively before we can assert its usefulness with precision.

V. CONCLUSION

The first global and kinetic study of $E \times B$ flows on the linear stability of ITG modes has been presented. It shows that:

- $E \times B$ flows have a very strong stabilizing effect on toroidal ITG modes.

- Only the intensity of the flow and its first derivative have an effect.
- For instance, the second derivative of flow (or curvature of flow) does not have any relevant effect.
- Negative magnetic shear does not enhance the effect of $E \times B$ flows.
- On the contrary, modes with positive magnetic shear are the most sensitive to $E \times B$ flows.
- Computed values are in qualitative and quantitative agreement with the only simulated experiment.

Acknowledgment: this work was in part supported by the Swiss National Science Foundation.

REFERENCES

[1] K.H. Burrell, Physics of Plasmas **4**, 1499, (1997)

[2] J.B. Taylor, H.R. Wilson, Plasma Phys. Control. Fusion **38**, 1999, (1996)

[3] M.Maccio, J. Vaclavik and L. Villard, in *Theory of Fusion Plasmas, Int. Workshop, Varenna, September 1998* (Editrice Compositori, Società Italiana di Fisica, Bologna, 1999), p.511

[4] T.S. Hahm, Physics of Plasmas **3**(12), 4658, (1996)

[5] S.Brunner, M. Fivaz, T.M. Tran and J. Vaclavik, Physics of Plasmas **5**(11), 3929, (1998)

[6] S.Brunner, J. Vaclavik, Physics of Plasmas **5**(2), 365, (1998)

[7] S. Brunner *et al.*, in *Theory of Fusion Plasmas, Int. Workshop, Varenna, August 1996* (Editrice Compositori, Società Italiana di Fisica, Bologna, 1996), p.101

[8] B. Davies, Jour. Comp. Phys., **66**, 36 (1986)

[9] M. Fivaz *et al.*, Comp. Phys. Comm., **111**, 27 (1998)

FIGURE CAPTIONS

Fig.1 No strong modification of the mode in the Fourier space when $E \times B$ flows are included. This case corresponds to a very strong physical effect: a stabilization by a factor three.

Fig.2 Scan in n to find the most unstable eigenmode of the system.

Fig.3 The three different shapes of $E \times B$ flow: $u(s)/s$ and $u(s)$.

Fig.4 Frequency as a function of Mach number, $\omega_{norm} = v_{thi}^2/[\omega_{ci}a^2]$. The 'circles' stand for the 'constant flow', the 'squares' for the 'constant shear' and the 'triangles' for the 'non-constant shear'.

Fig.5 Growth rate as a function of Mach number. The 'circles' stand for the 'constant flow', the 'squares' for the 'constant shear and the 'triangles' for the 'non-constant shear'.

Fig.6 Benchmark with local dispersion relation and PIC code.

Fig.7 Contours of ITG mode in the poloidal plane for various Mach numbers. On the left is the Constant Flow case, while on the right is the Constant Shear case.

Fig.8 $k_\perp$ and $k_\parallel$ as functions of Mach number. The 'circles' stand for the 'constant flow' and the 'triangles' for the 'constant shear'.

Fig.9 Poloidal contours of the ITG modes for the three considered values of magnetic shear.

Fig.10 Evolution of the complete spectrum in the complex plane (in units of ω_{norm}) as a function of Mach number, for the three magnetic shear cases. Each '+' represents an eigenvalue.

Fig.11 Evolution of the most unstable mode for the three considered values of magnetic shear, as a function of Mach number. Circles, squares and diamonds respectively represent the negative, zero and positive magnetic shear cases.

Fig.12 Important equilibrium profiles of Asdex Upgrade.

Fig.13 Spectrum of the AUG case (without $E \times B$ flows) with and without trapped electrons (TE). The circles and squares are the results of the local dispersion relation, with $\tau = T_e/T_i$ varying from 1 to 0.3 for both cases: with and without TE. the triangles are the evolution of the most unstable global mode without TE and with τ varying from 1 to 0.4. Finally the diamond is the most unstable global mode with TE included, for the experimental value of $\tau = 0.332$. Variations of τ are obtained through the variation of T_e.

Fig.14 Complete spectrum of the microinstabilities of the AUG case, for various value of Mach number: circles are global results without flow, while squares and triangles represent increasing values of Mach number.

Fig.15 Most unstable mode of the AUG spectrum, without and with $E \times B$ flow.

FIGURES

FIG.1 Maccio

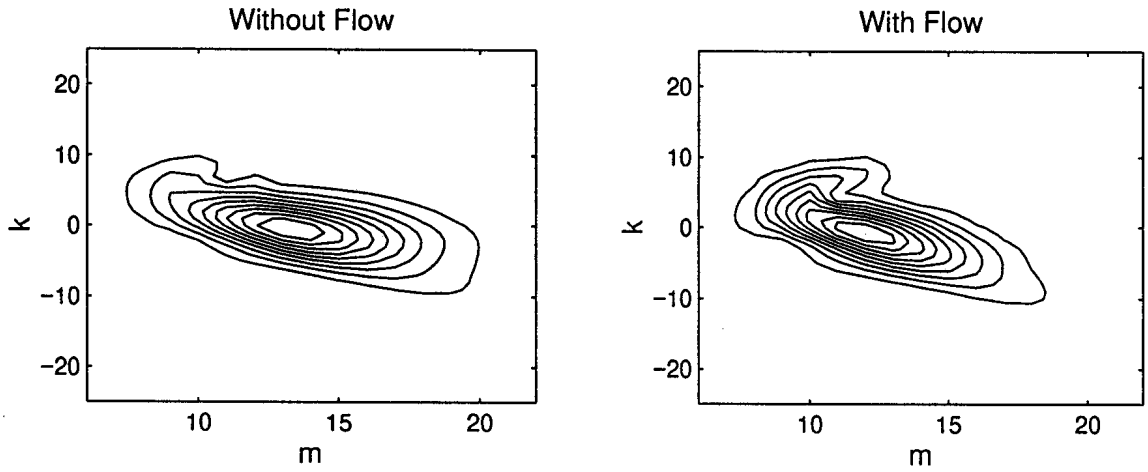

FIG.2 Maccio

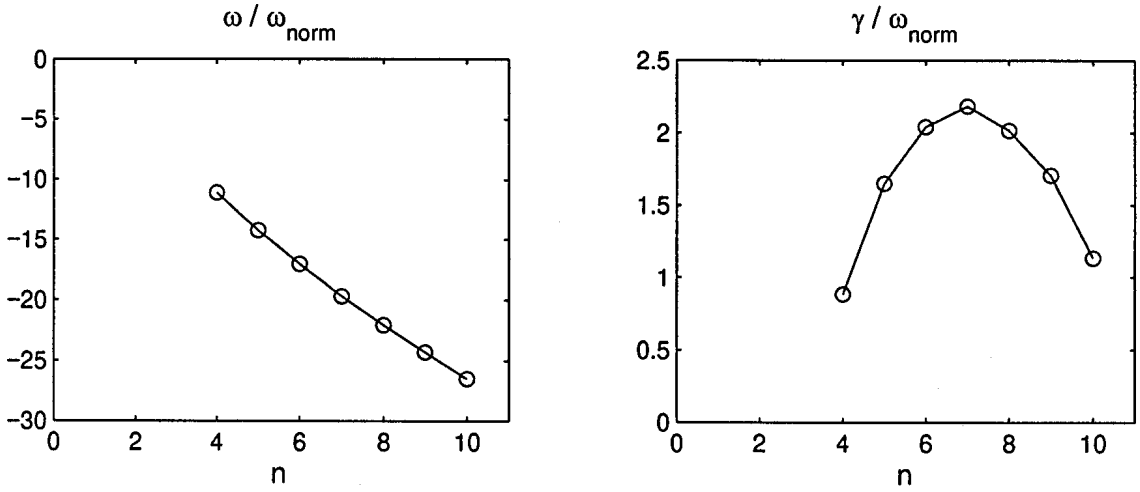

FIG.3 Maccio

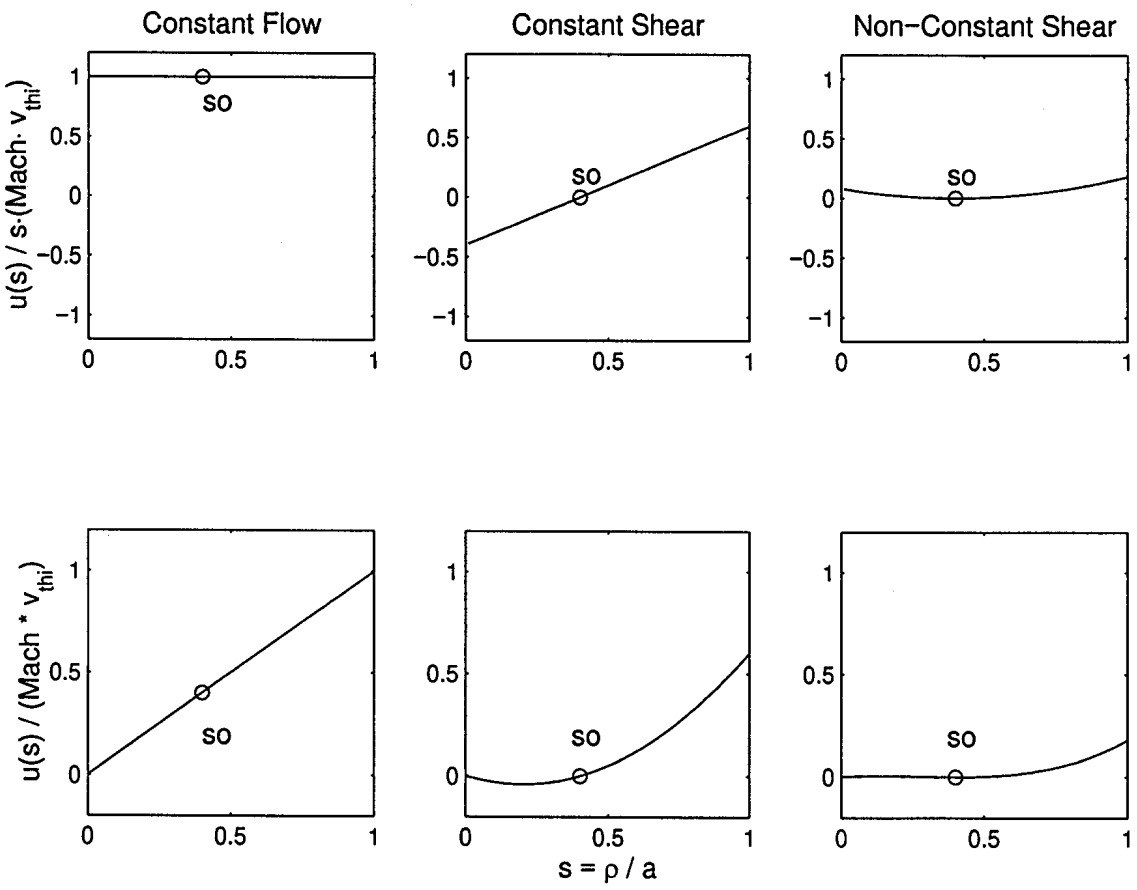
Constant Flow
Constant Shear
Non−Constant Shear
u(s) / s·(Mach· v_thi)
u(s) / (Mach * v_thi)
so
s = ρ / a

FIG.4 Maccio

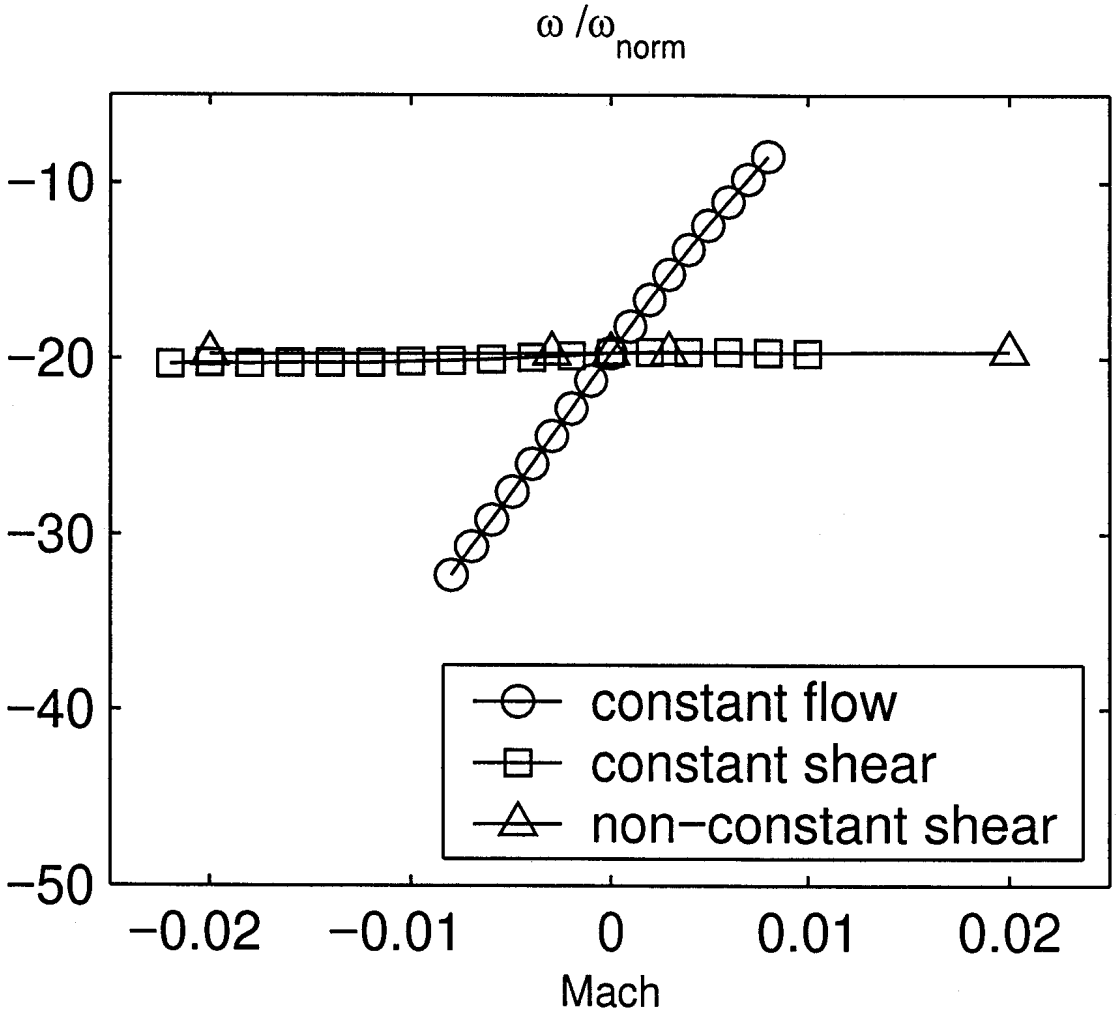
ω /ω norm
−10
−20
−30
−40
−50
−0.02
−0.01
0
0.01
0.02
Mach
constant flow
constant shear
non−constant shear

FIG.5 Maccio

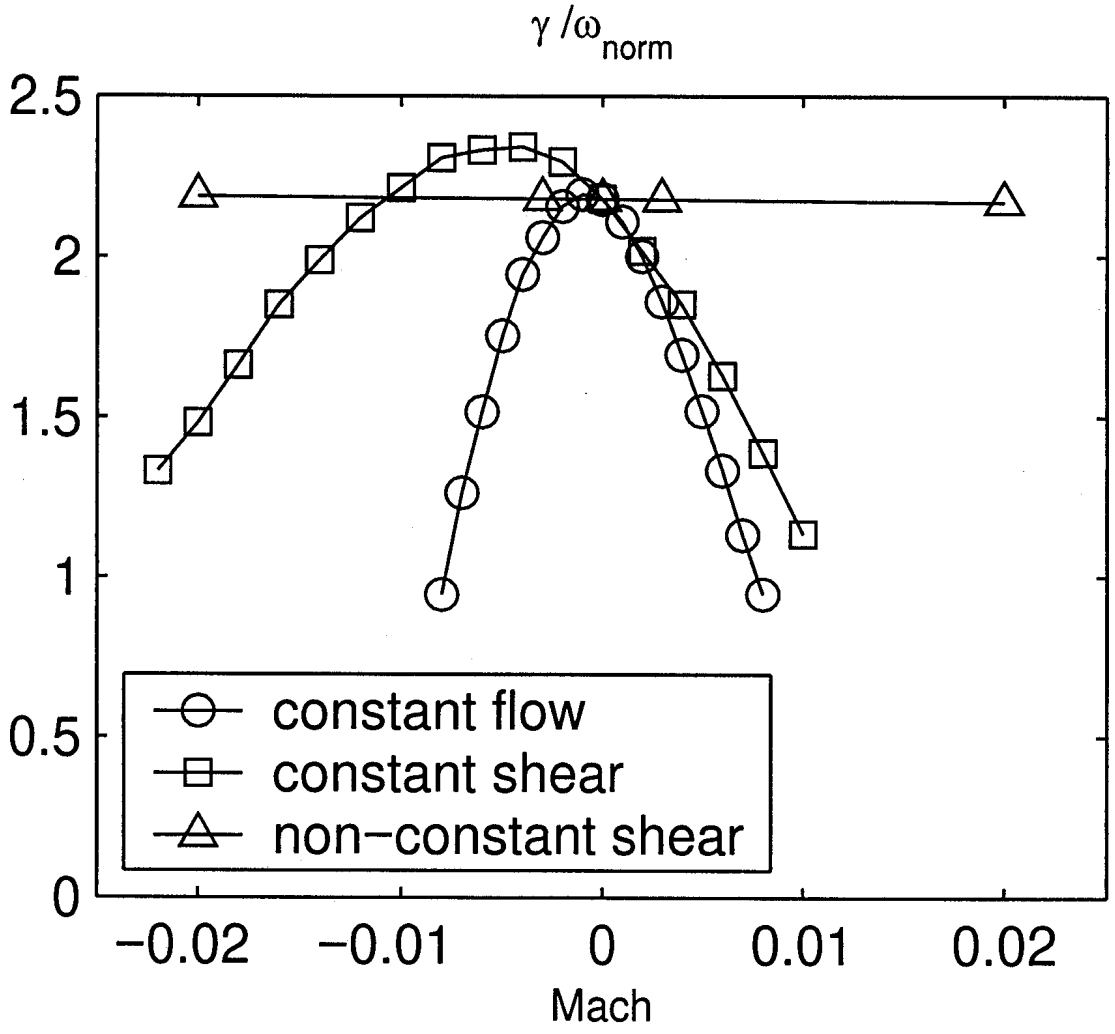
γ /ω norm
2.5
2
1.5
1
0.5
0
−0.02
−0.01
0
0.01
0.02
Mach
constant flow
constant shear
non−constant shear

FIG.6 Maccio

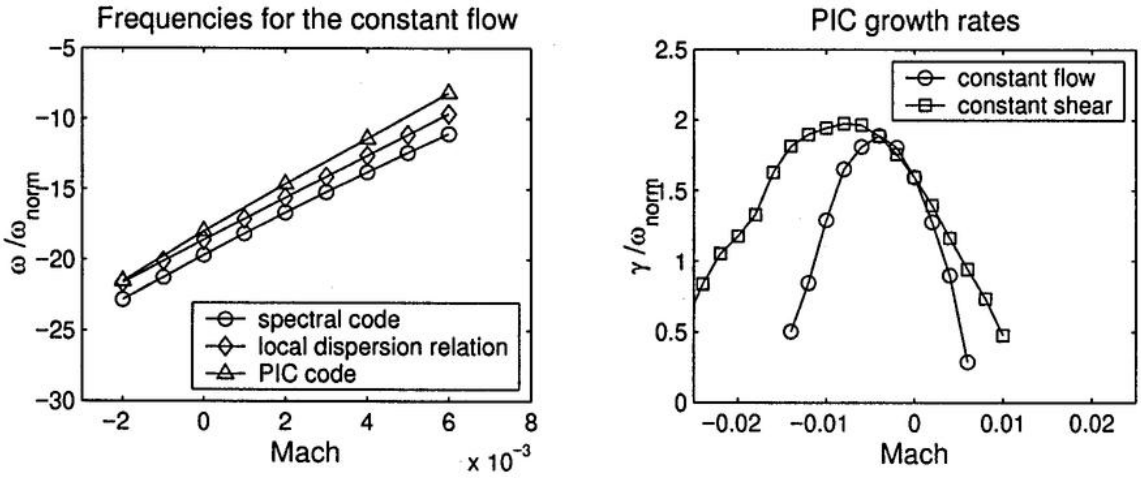
Frequencies for the constant flow
ω /ω norm
−5
−10
−15
−20
−25
−30
−2
0
2
4
6
8
Mach
x 10^−3
spectral code
local dispersion relation
PIC code
PIC growth rates
γ /ω norm
2.5
2
1.5
1
0.5
0
−0.02
−0.01
0
0.01
0.02
Mach
constant flow
constant shear

FIG.7 Maccio

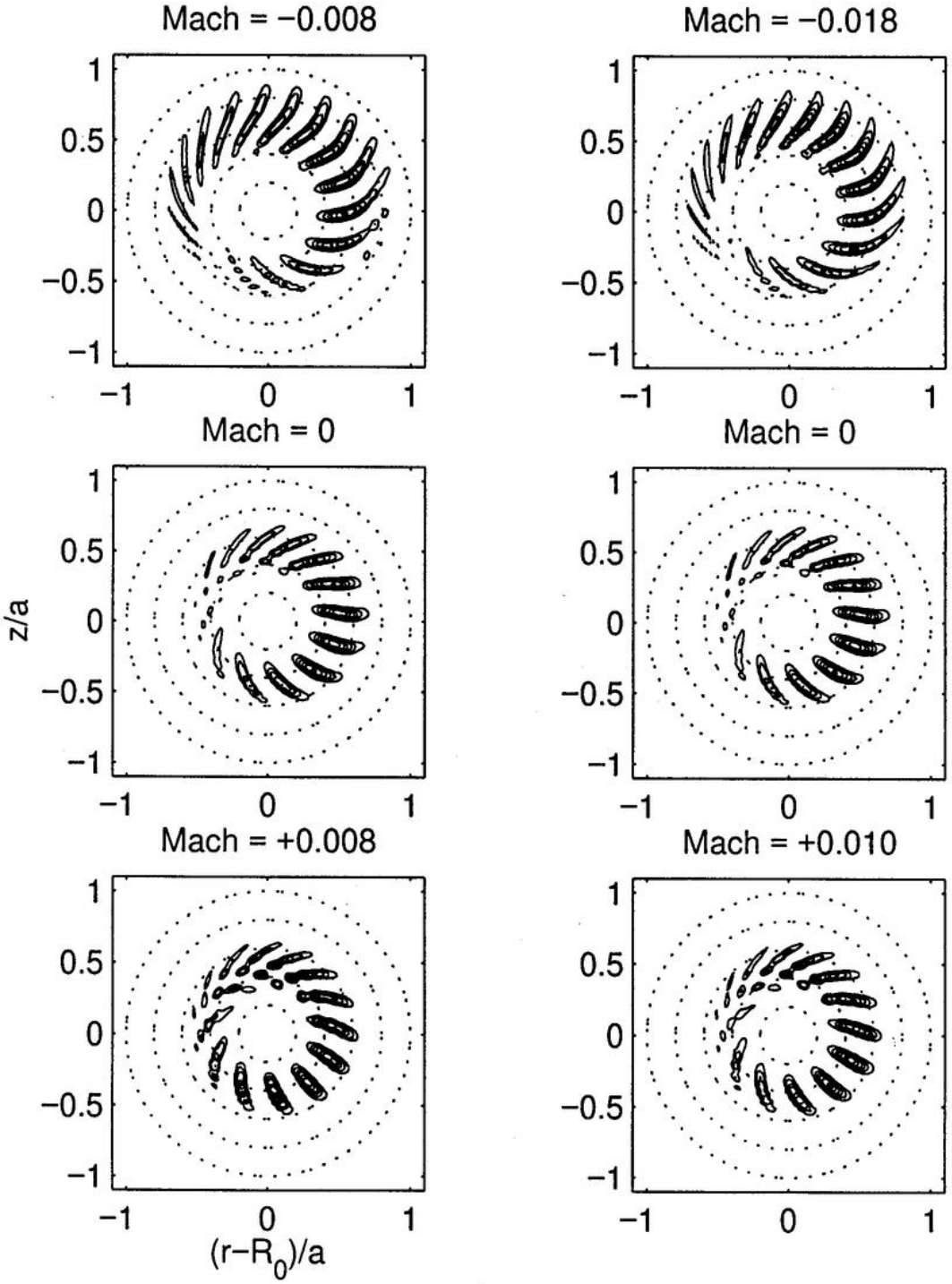
Mach = −0.008
Mach = −0.018
Mach = 0
Mach = 0
Mach = +0.008
Mach = +0.010
z/a
(r−R0)/a
1
0.5
0
−0.5
−1

FIG.8 Maccio

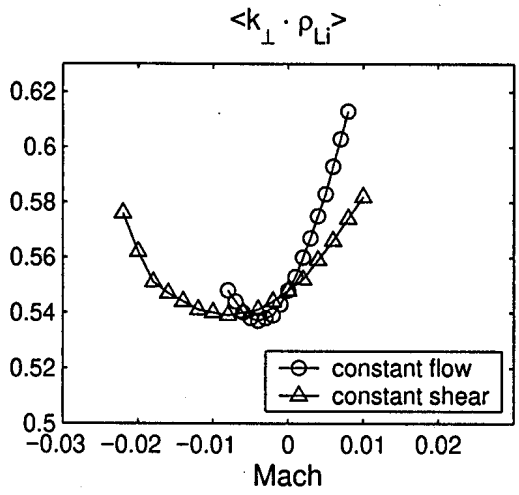
<k⊥ · ρLi>
0.62
0.6
0.58
0.56
0.54
0.52
0.5
−0.03 −0.02 −0.01 0 0.01 0.02
Mach
constant flow
constant shear

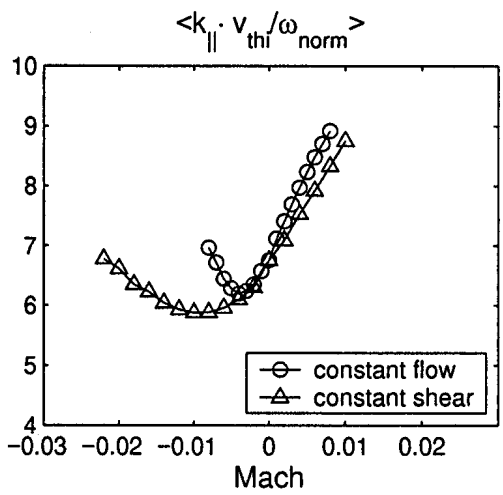
<k|| · vthi/ωnorm>
10
9
8
7
6
5
4
−0.03 −0.02 −0.01 0 0.01 0.02
Mach
constant flow
constant shear

FIG.9 Maccio

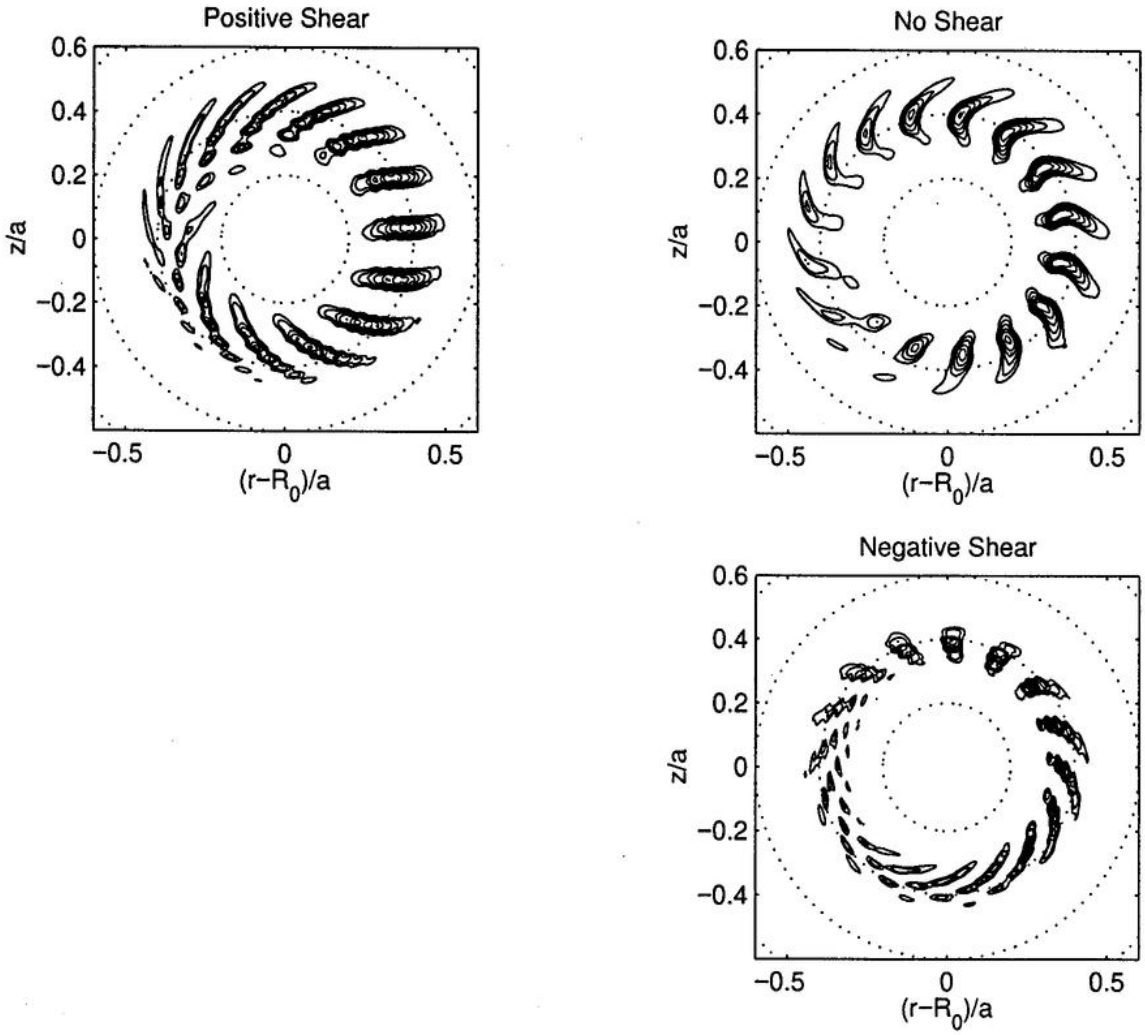
Positive Shear
No Shear
Negative Shear
z/a
(r−R0)/a
0.6
0.4
0.2
0
−0.2
−0.4
−0.5
0
0.5

FIG.10 Maccio

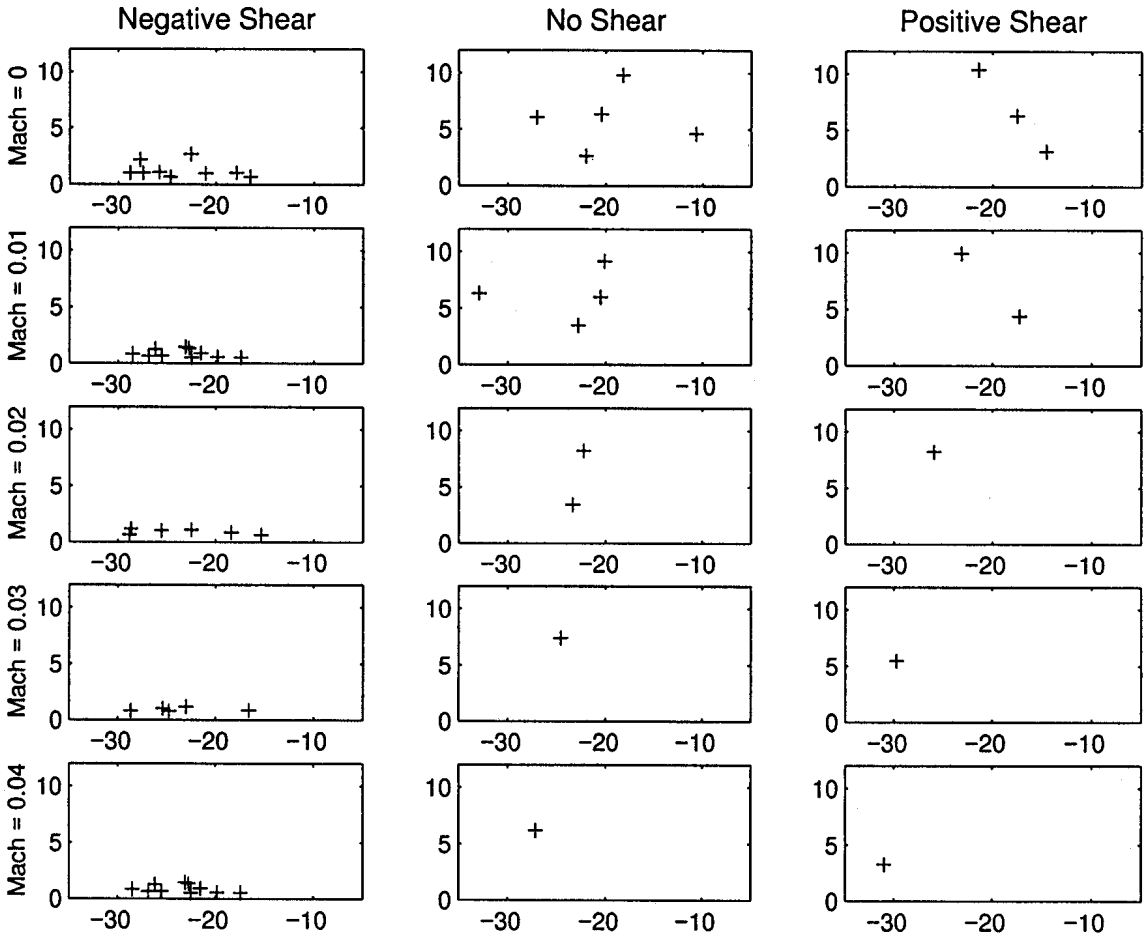

FIG.11 Maccio

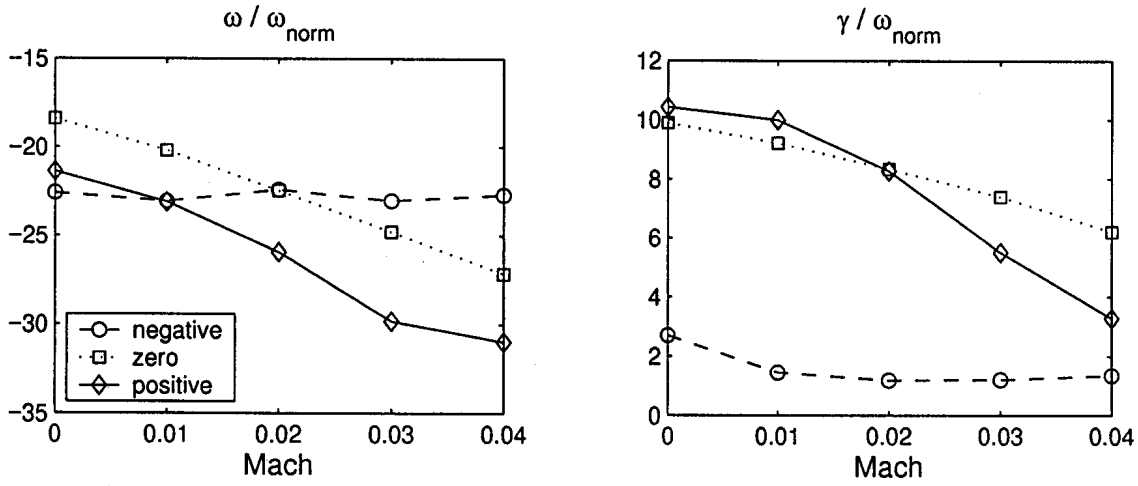

FIG.12 Maccio

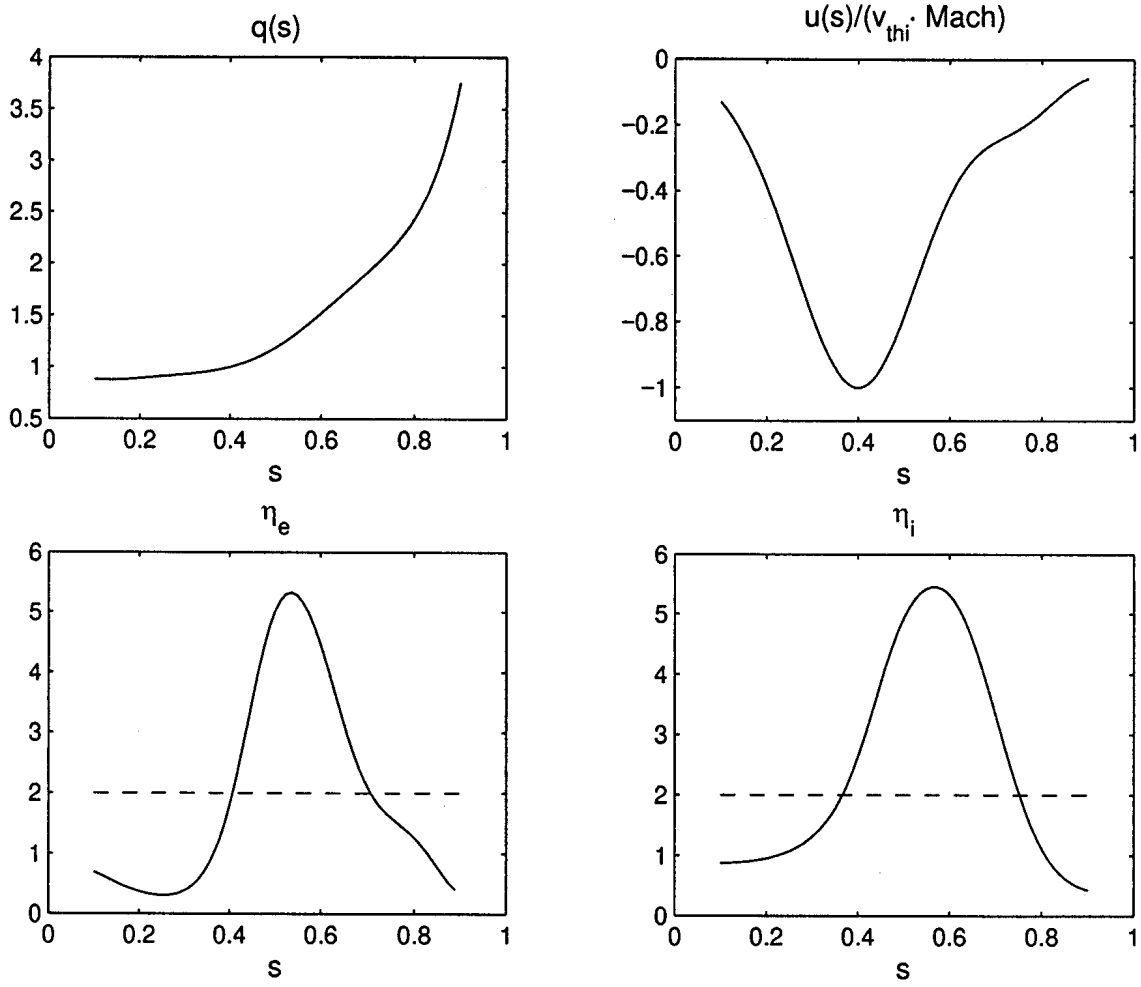

FIG.13 Maccio

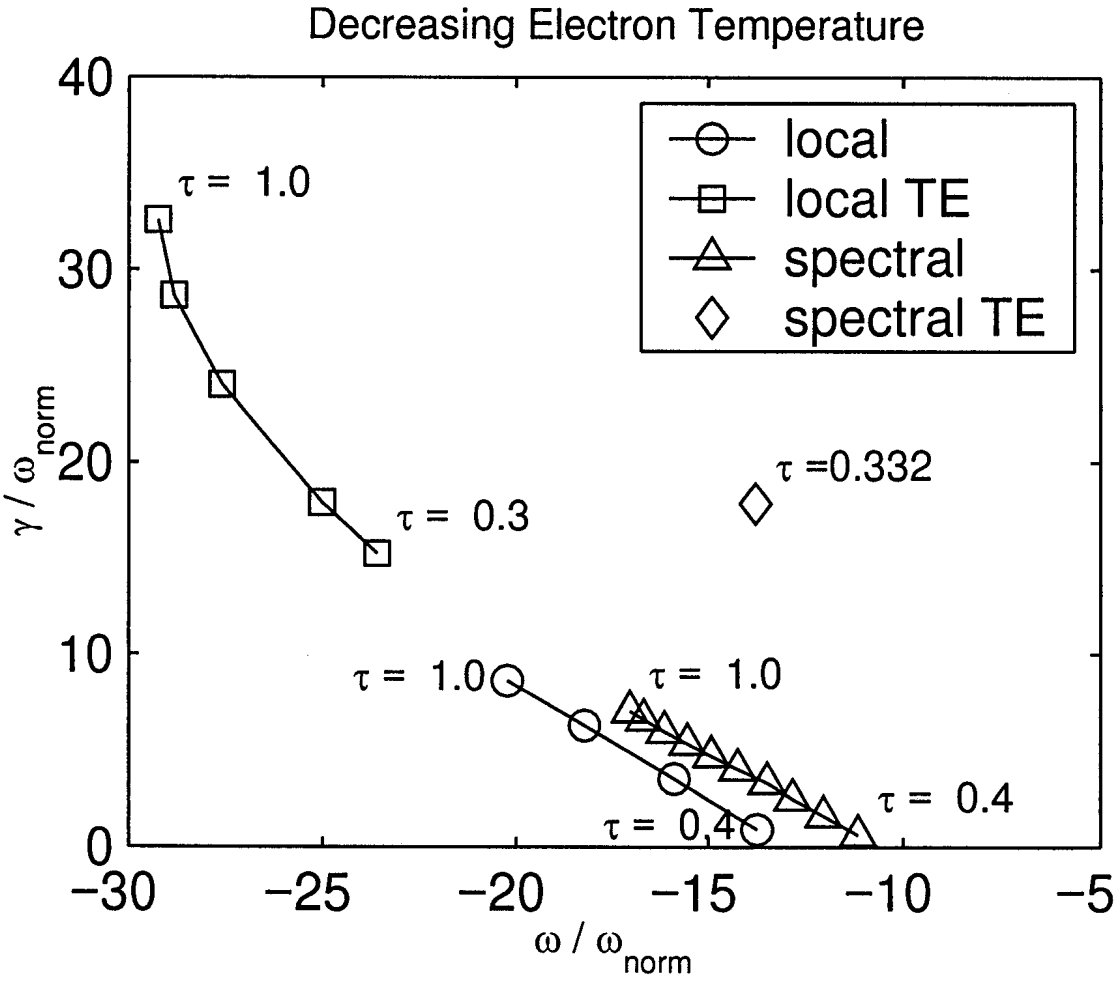

FIG.14 Maccio

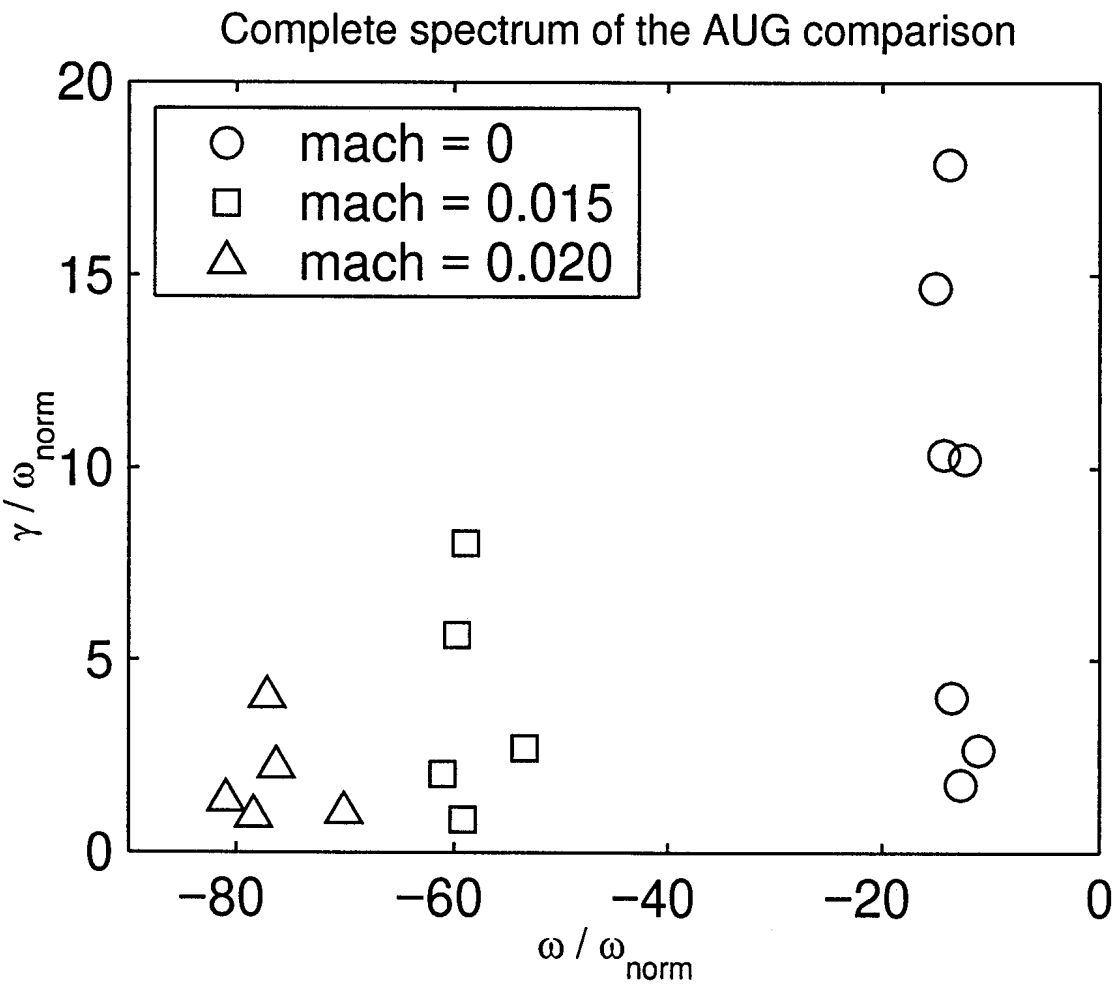

FIG.15 Maccio